


# Aromaticity at position 39 in $\alpha$ -synuclein: A modulator of amyloid fibril assembly and membrane-bound conformations

Fiamma A. Buratti<sup>1</sup> | Nicola Boeffinger<sup>2,3</sup> | Hugo A. Garro<sup>1,4</sup> |  
 Jesica S. Flores<sup>1</sup> | Francisco J. Hita<sup>1</sup> | Phelippe do Carmo Gonçalves<sup>1</sup> |  
 Federico dos Reis Copello<sup>5</sup> | Leonardo Lizarraga<sup>5</sup> | Giulia Rossetti<sup>6,7,8</sup> |  
 Paolo Carloni<sup>6,9,10</sup> | Markus Zweckstetter<sup>2,11</sup> | Tiago F. Outeiro<sup>12,13,14</sup> |  
 Stefan Eimer<sup>3</sup> | Christian Griesinger<sup>2</sup> | Claudio O. Fernández<sup>1,2</sup> 

<sup>1</sup>Max Planck Laboratory for Structural Biology, Chemistry and Molecular Biophysics of Rosario (MPLbioR, UNR-MPINAT), Partner Laboratory of the Max Planck Institute for Multidisciplinary Sciences (MPINAT, MPG). Centro de Estudios Interdisciplinarios, Universidad Nacional de Rosario, Rosario, Argentina

<sup>2</sup>Department of NMR-based Structural Biology, Max Planck Institute for Multidisciplinary Sciences, Göttingen, Germany

<sup>3</sup>Department of Structural Cell Biology, Institute for Cell Biology and Neuroscience, Goethe University Frankfurt, Frankfurt, Germany

<sup>4</sup>Area de Química Orgánica, UNSL-INTEQUI/CONICET, San Luis, Argentina

<sup>5</sup>Centro de Investigaciones en Bionanociencias (CIBION-CONICET), Buenos Aires, Argentina

<sup>6</sup>Computational Biomedicine, Institute for Neuroscience and Medicine (INM-9) and Institute for Advanced Simulations (IAS-5), Jülich, Germany

<sup>7</sup>Department of Neurology, University Hospital Aachen, RWTH Aachen University, Aachen, Germany

<sup>8</sup>Jülich Supercomputing Center (JSC), Jülich, Germany

<sup>9</sup>Faculty of Mathematics, Computer Science and Natural Sciences, RWTH Aachen, Aachen, Germany

<sup>10</sup>Institute for Neuroscience and Medicine (INM-11) Forschungszentrum Jülich, Jülich, Germany

<sup>11</sup>German Center for Neurodegenerative Diseases (DZNE), Göttingen, Germany

<sup>12</sup>Department of Experimental Neurodegeneration, Center for Biostructural Imaging of Neurodegeneration, University Medical Center Göttingen, Göttingen, Germany

<sup>13</sup>Translational and Clinical Research Institute, Newcastle University, Newcastle, UK

<sup>14</sup>Scientific employee with an honorary contract at Deutsches Zentrum für Neurodegenerative Erkrankungen (DZNE), Göttingen, Germany

## Correspondence

Claudio O. Fernández. Max Planck Laboratory for Structural Biology, Chemistry and Molecular Biophysics of Rosario (MPLbioR, UNR-MPINAT). Partner Laboratory of the Max Planck Institute for Multidisciplinary Sciences (MPINAT, MPG), Göttingen, Germany. Centro de Estudios Interdisciplinarios, Universidad Nacional de Rosario, Riobamba y Berutti, S2002LRK Rosario, Argentina.

## Abstract

Recent studies revealed that molecular events related with the physiology and pathology of  $\alpha$ S might be regulated by specific sequence motifs in the primary sequence of  $\alpha$ S. The importance of individual residues in these motifs remains an important open avenue of investigation. In this work, we have addressed the structural details related to the amyloid fibril assembly and lipid-binding features of  $\alpha$ S through the design of site-directed mutants at position 39 of the protein and their study by in vitro and in vivo assays. We demonstrated that aromaticity at position 39 of  $\alpha$ S primary sequence influences strongly the

This is an open access article under the terms of the [Creative Commons Attribution-NonCommercial](https://creativecommons.org/licenses/by-nc/4.0/) License, which permits use, distribution and reproduction in any medium, provided the original work is properly cited and is not used for commercial purposes.

© 2022 The Authors. *Protein Science* published by Wiley Periodicals LLC on behalf of The Protein Society.

Email: [cfernandez@cei-mplbior.unr.edu.ar](mailto:cfernandez@cei-mplbior.unr.edu.ar); [cfernan@mpinat.mpg.de](mailto:cfernan@mpinat.mpg.de)

#### Funding information

Michael J. Fox Foundation, Grant/Award Number: 019033; EU Horizon 2020; Deutsche Forschungsgemeinschaft, Grant/Award Number: 2067/1-390729940; Max Planck Society, Grant/Award Number: P10390; Universidad Nacional de Rosario; ANPCyT-FONCYT PICT, Grant/Award Number: 2017-4665; Alexander von Humboldt Foundation

**Review Editor:** Hideo Akutsu

aggregation properties and the membrane-bound conformations of the protein, molecular features that might have important repercussions for the function and dysfunction of  $\alpha$ S. Considering that aggregation and membrane damage is an important driver of cellular toxicity in amyloid diseases, future work is needed to link our findings with studies based on toxicity and neuronal cell death.

**Brief statement outlining significance:** Modulation by distinct sequential motifs and specific residues of  $\alpha$ S on its physiological and pathological states is an active area of research. Here, we demonstrated that aromaticity at position 39 of  $\alpha$ S modulates the membrane-bound conformations of the protein, whereas removal of aromatic functionality at position 39 reduces strongly the amyloid assembly *in vitro* and *in vivo*. Our study provides new evidence for the modulation of molecular events related with the physiology and pathology of  $\alpha$ S.

#### KEYWORDS

amyloid fibril, fluorescence and confocal microscopy, lipid interaction, NMR, sequence motifs,  $\alpha$ -synuclein

## 1 | INTRODUCTION

Alpha-synuclein ( $\alpha$ S) is a disordered, neuronal cytoplasmic protein located predominantly at the presynaptic termini of the central nervous system.<sup>1</sup> Misfolding and aberrant aggregation of  $\alpha$ S is associated with neuropathological disorders collectively referred to as synucleinopathies.<sup>2–8</sup> Although the physiological functions of  $\alpha$ S remain elusive, it has been implicated in synaptic plasticity<sup>9</sup> and maintenance of synaptic vesicle pool size.<sup>10,11</sup> Strikingly, despite strong efforts over the years, the precise mechanisms leading to  $\alpha$ S aggregation are unclear.

The primary structure of  $\alpha$ S comprises 140 amino acids distributed in three regions: the amphipathic N-terminus (residues 1–60), implicated in lipid binding<sup>12</sup>; the central region, known as NAC (residues 61–95), which is highly hydrophobic and fibrillogenic<sup>13,14</sup>; and the acidic C-terminus (residues 96–140), critical for blocking rapid  $\alpha$ S filament assembly.<sup>15–17</sup> Whereas in its free monomeric state,  $\alpha$ S adopts an ensemble of disordered, aggregation-autoinhibited conformations,<sup>18–20</sup> upon binding to lipid membranes, the protein undergoes a disorder-to-helix transition in the N-terminal, encompassing the first 100 amino acids.<sup>21</sup>

Systematic analysis of the role of distinct sequential motifs and specific residues of  $\alpha$ S primary sequence on its physiological and pathological states remains an important open avenue of investigation. Studies focused on  $\alpha$ S mutations, post-translational modifications, and molecular interactions are emerging as of central importance to

the normal function of the protein, as well as to its pathogenic role in Parkinson disease.<sup>22–34</sup> In this context, a segment of 12 residues at the amino-terminus as well as a region surrounding Tyr-39 were identified recently as canonical chaperone interaction motifs of  $\alpha$ S in mammalian cells, through which molecular chaperones might prevent the transformation of  $\alpha$ S towards pathological states.<sup>22,25</sup> In parallel, other studies showed that the region consisting of residues 36–42 is important in promoting  $\alpha$ S aggregation.<sup>27,32</sup> Added to that, post-translational modifications at Tyr-39 were suggested to play a role in the physiology and pathology of  $\alpha$ S.<sup>22–26,30,31,33,34</sup>

In the frame of our studies in the field of the structural biology of Parkinson disease, we recently showed that removing aromaticity at position 39 affects the compactness of the protein and impacts strongly on the inhibitory interaction of  $\alpha$ S with amyloid-blocking agents.<sup>35–37</sup> In this work, we have addressed structural details related to the aggregation and lipid-binding features of  $\alpha$ S and its site-directed mutants Y39F, Y39L, and Y39A  $\alpha$ S. By the characterization of the amyloid assembly of these species *in vitro* and *in vivo*, and the analysis of its conformations in the membrane-bound state, we can draw the following conclusions: (i) removal of aromatic residues at position 39 impairs the *in vitro* amyloid fibril assembly of  $\alpha$ S; (ii) the aggregation propensity of  $\alpha$ S is also affected by the aromaticity at position 39 in cell-based assays and animal models; and (iii) aromaticity at position 39 determines the membrane-bound conformation of  $\alpha$ S by

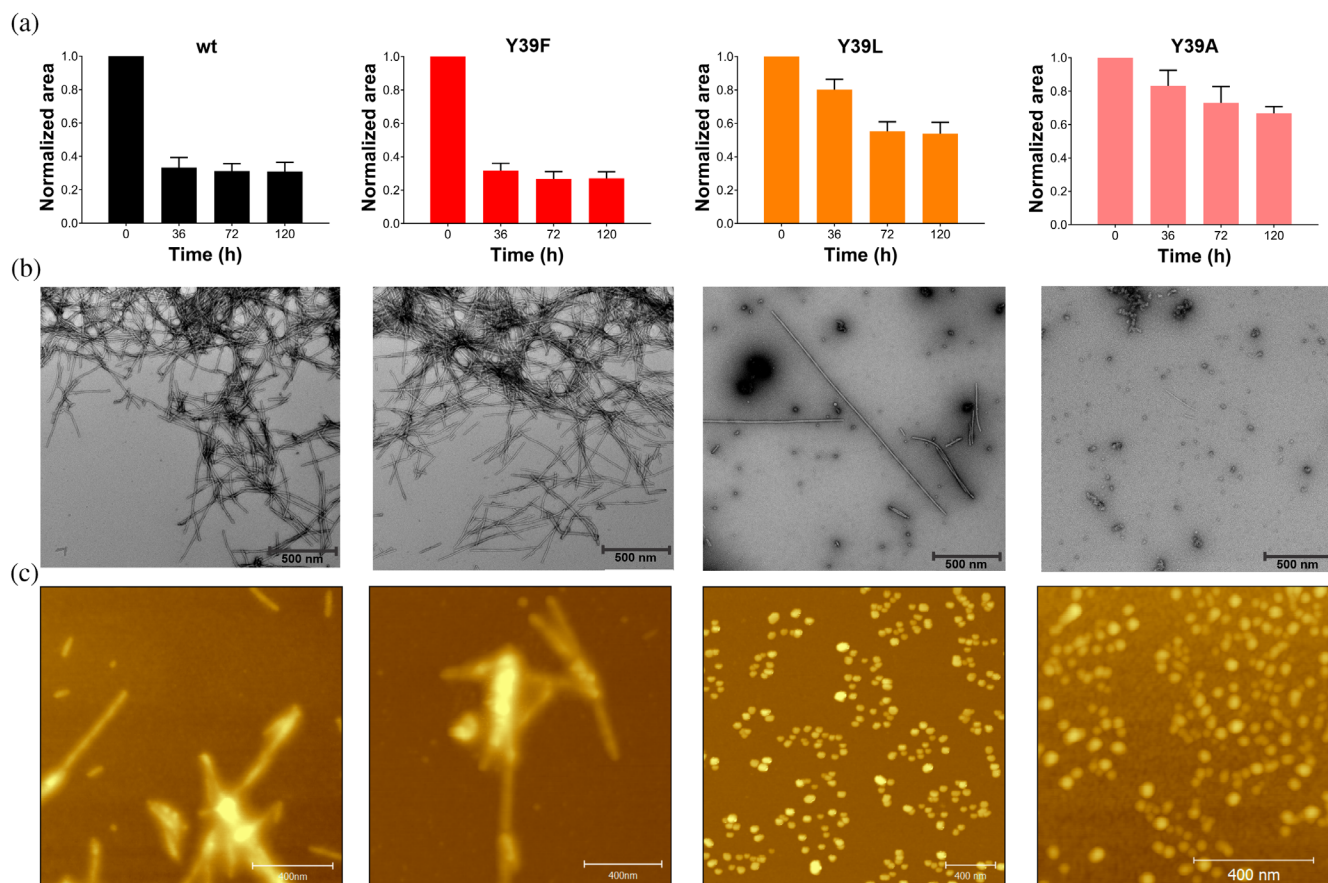


**FIGURE 1** Effects of Y39 mutations on  $\alpha$ S fibril formation. (a) Level of remaining soluble  $\alpha$ S monomers determined by 1D  $^1\text{H}$ -NMR as a function of aggregation time. (b) Representative negative-stain electron microscopy images of  $\alpha$ S aggregates (50  $\mu\text{M}$  samples) taken at 120 hr. Scale bars, 500 nm. (c) AFM of  $\alpha$ S aggregates (50  $\mu\text{M}$  samples) after 120 hr incubation. Scale bars, 400 nm

modulating lipid interactions involving the central hydrophobic NAC domain.

## 2 | RESULTS

### 2.1 | Removal of aromaticity at position 39 impairs the *in vitro* amyloid fibril assembly of $\alpha$ S

We evaluated first the amyloid-forming capability of the different  $\alpha$ S species. As shown in Figure 1a, the time course of aggregation of wt  $\alpha$ S monitored as monomer consumption by 1D  $^1\text{H}$ -NMR spectroscopy was comparable to that measured for the Y39F mutant, whereas those species containing the Y39L and Y39A mutation showed a significant reduction in the rate and amount of aggregated protein (1A). Results consistent to those reported by NMR were independently obtained when circular dichroism (CD) and the amyloid-sensitive Thioflavin T (ThT) fluorescence assay were used to determine the

change in secondary structure content of  $\alpha$ S species during fibril assembly (Figure S1a-b).

The morphology of the aggregation products of the  $\alpha$ S variants was then characterized by transmission electron microscopy (TEM). Ultrastructural visualization of the protein deposits obtained for the Y39F species revealed the presence of abundant amounts of typical amyloid fibrils that were morphologically indistinguishable from those formed for the wild-type protein (Figure 1b). In contrast, the TEM images corresponding to the Y39L and Y39A species showed predominantly nonfibrillar protein structures (Figure 1b), with a minuscule amount of isolated fibrillar components detectable only for the Y39L variant (1C).

To further characterize the structures observed in electron micrographs, atomic force microscopy (AFM) was performed. As shown in Figure 1c, samples of wild-type and Y39F aggregates are comprised of typical amyloid fibrils. In contrast, AFM images of the final products of aggregation of Y39L and Y39A resulted mostly in the formation of nonfibrillar, spheroid-like aggregates.

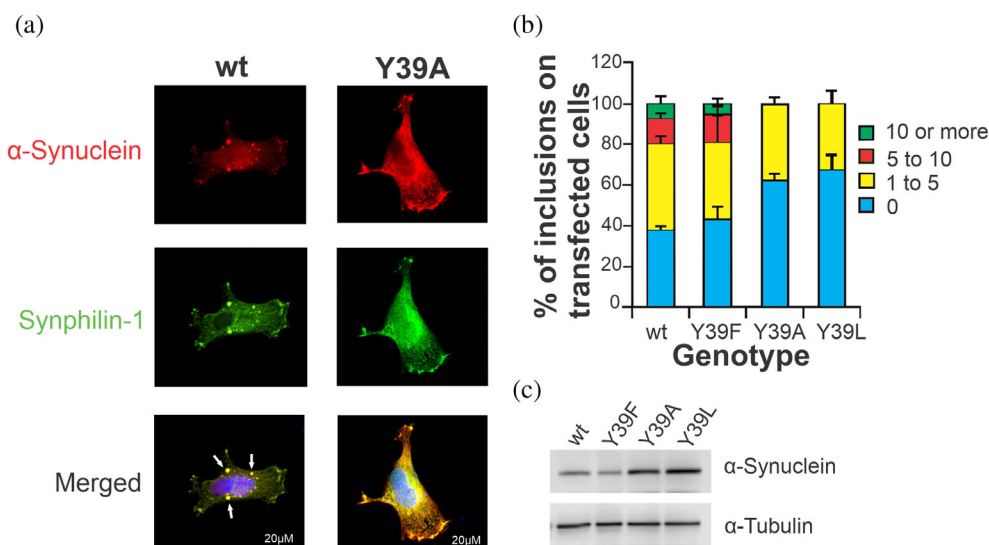


**FIGURE 2** Modulation of  $\alpha$ S inclusion formation in cultured cells. (a) Representative images of intracellular wt and Y39A  $\alpha$ S inclusion formation in human cultured cells. Scale bars, 20  $\mu$ m. (b) Quantification of  $\alpha$ S inclusions. Transfected cells were classified in different groups: 1 to 4, 5 to 9, and equal to/more than 10 inclusions. Results were expressed as the percentage of the total number of transfected cells obtained from three independent experiments. At least 50 cells were scored per experiment ( $n = 3$ ). (c) Immunoblot analysis of the expression levels of the  $\alpha$ S variants studied in H4 cells

Altogether, these results demonstrate that mutations Y39L and Y39A impair the *in vitro* amyloid fibril assembly of  $\alpha$ S.

## 2.2 | The aggregation propensity of $\alpha$ S in biological models is affected by the aromaticity at position 39

The next question was whether the *in vitro* findings are corroborated by the behavior of the mutant proteins in the context of a mammalian cell model. To address this question, we assessed the effect of mutations at position 39 in a well-established cell model that leads to positive intracellular protein inclusion formation for  $\alpha$ S.<sup>38</sup> Treatment with  $\alpha$ S promoted a significant number of transfected cells displaying  $\alpha$ S inclusions (Figure 2a), while analysis of protein inclusion formation in the Y39F transfected cells showed a pattern comparable to that of wt  $\alpha$ S (Figure 2b). In contrast, for the Y39L and Y39A variants, we observed a significant decrease in the percentage of cells with inclusions (Figure 2a-b). To investigate whether these effects might be explained by differences in the levels of  $\alpha$ S being expressed, we performed immunoblot analysis. There was no correlation between the expressed levels of the studied proteins and inclusions formation, indicating that the results were intimately correlated with the effects of the mutations on aggregation (Figure 2c).

Next, to corroborate the results in postmitotic neurons, we used the nematode *C. elegans* as a multicellular

model system to study the aggregation of  $\alpha$ S variants at position 39.<sup>39</sup> When expressed in motoneurons as a C-terminal fusion with mCherry, wt or Y39F  $\alpha$ S mutant formed numerous large aggregates (Figure 3a-b). By contrast, the number and size of these aggregates were reduced when Y39L or Y39A mutant forms of  $\alpha$ S were expressed (Figure 3a-b). Like in the cell model, the observed differences in aggregation were not due to differences in expression levels of  $\alpha$ S as quantified by Western blot experiments (Figure 3c).

Overall, the results obtained in culture cells and *C. elegans* neurons demonstrate that intracellular inclusions of  $\alpha$ S are significantly reduced when Y39L and Y39A  $\alpha$ S variants were expressed as compared to wt or Y39F  $\alpha$ S variants. This strongly suggests that like *in vitro*, the aggregation propensity of  $\alpha$ S is also affected by the aromaticity at position 39 *in vivo*.

## 2.3 | Aromaticity at position 39 is a determinant of the membrane-bound conformation of $\alpha$ S

Since the association of  $\alpha$ S with cellular membranes and changes in those interactions might have functional and pathological implications, we also investigated the effect of mutations at Y39 on the binding features of  $\alpha$ S to lipid-vesicles (small unilamellar vesicles: SUVs). Changes in  $\alpha$ S structure associated with membrane binding were monitored by far-UV CD,

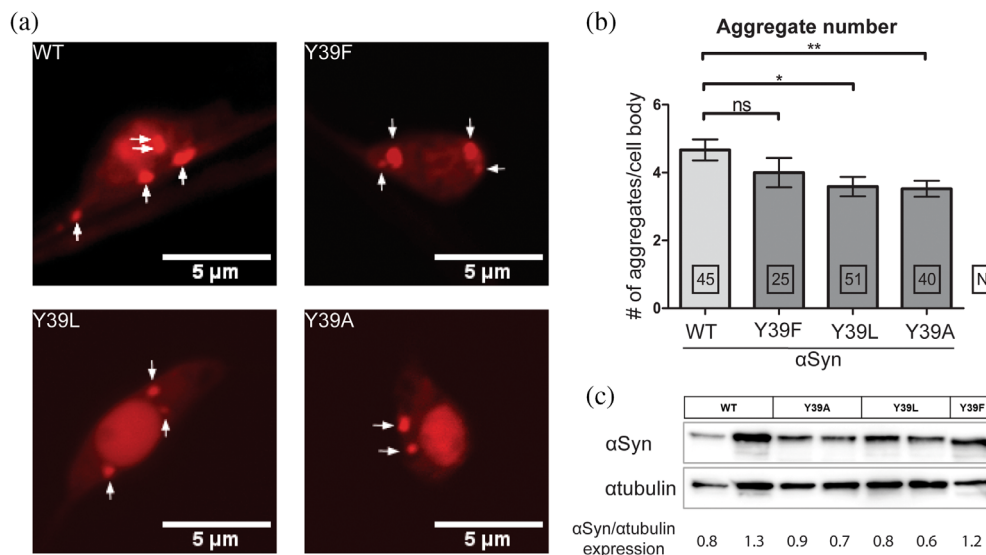


**FIGURE 3** Aggregation of  $\alpha$ S in *C. elegans* motoneurons is affected by the aromaticity at position 39. (a) Confocal images of one day adult motoneurons showing the formation of intracellular  $\alpha$ S-mCherry aggregates. Scale bars, 5  $\mu$ m. (b) Quantification of intracellular  $\alpha$ S aggregates. The values shown represent the mean  $\pm$  SEM; for comparison an unpaired, two-tailed *t*-test was used; \* and \*\* denote  $p < 0.05$  and 0.01, respectively. (c) Total  $\alpha$ S expression levels were quantified by Western blot experiments relative to  $\alpha$ Tubulin loading control

which reports on the increase in  $\alpha$ S  $\alpha$ -helicity upon interaction with phospholipids.<sup>28</sup> The far-UV CD spectra of  $\alpha$ S is characterized by a minimum at 198 nm in the absence of SUVs, whereas a maximum at 192 nm and minima at 208 nm and 222 nm are typical of its membrane-bound state. CD spectra for the wt and Y39A  $\alpha$ S species in the presence of varying concentrations of SUVs are shown in Figure 4a-b. To compare the binding affinities of  $\alpha$ S and its Y39F, Y39L, and Y39A variants to SUVs, the mean residue molar ellipticity at 222 nm ( $[\theta]_{MR,222}$ ) for all species was monitored as a function of lipid concentration (Figure 4c). In all cases, analysis of the titration data yielded  $K_d$  values in the 0.1–0.2  $\mu$ M range.

To explore the structural details of the binding, we used NMR spectroscopy. The <sup>15</sup>N-labeled  $\alpha$ S mutants were analyzed by 2D <sup>1</sup>H–<sup>15</sup>N HSQC spectra recorded in the absence or presence of SUVs. This assay provides a residue-by-residue readout of lipid binding that is useful to evaluate which residues on the protein are in greatest contact with the vesicle.<sup>40</sup> NMR experiments correlate the normalized signal attenuation of resonances from specific residues, obtained in the presence of SUV, to the binding of these residues to the membrane. For each residue of  $\alpha$ S,  $I/I_0$  is the proportion of molecules in an  $\alpha$ S/SUV mixture in which the residue remains mobile and in solution, and the fractional attenuation ( $1 - I/I_0$ ) is the proportion of molecules in which the residue is tightly associated with the membrane.<sup>40</sup> We used this approach to characterize the  $\alpha$ S–membrane interaction, in particular, to determine the fractional population of molecules

bound to the membrane (“total bound population”) and whether the central hydrophobic (aggregation-prone) region was either dissociated or associated in the case of conformers referred as “exposed” or “hidden,” respectively.<sup>28</sup> The fractional population of molecules bound to the membrane in either mode was determined from the mean attenuation of residues 3–9, based on the fact that the N-terminal segment of  $\alpha$ S has a higher membrane affinity compared to more C-terminal regions<sup>41</sup> and is lipid-bound in the case of both exposed and hidden conformers.<sup>40</sup> Regarding the conformation of the hydrophobic domain NAC at the membrane, which is described to have an important role in the regulation of biological properties of  $\alpha$ S and on its oligomerization,<sup>42,43</sup> the fractional population of protein in the hidden state was determined by measuring the mean attenuation of residues 66–80,<sup>28</sup> a segment that plays a key role in  $\alpha$ S self-assembly.<sup>14</sup> On the other hand, the fractional population of protein with residues 66–80 in the exposed state was determined by subtracting the hidden population from the total bound population (residues 3–9).<sup>28</sup>

As shown in Table 1, the  $\alpha$ S mutants exhibited nearly the same total populations for their membrane-bound states. However, clear structural differences were observed among the vesicle-bound forms of the  $\alpha$ S variants at the level of the hydrophobic NAC domain. Our results indicate that the percentage of total bound molecules with the hydrophobic NAC in a membrane-dissociated state was increased by a factor of 1.7 and 2.0 in the cases of the Y39L and Y39A variants compared to wt and Y39F. This means that aromaticity at position

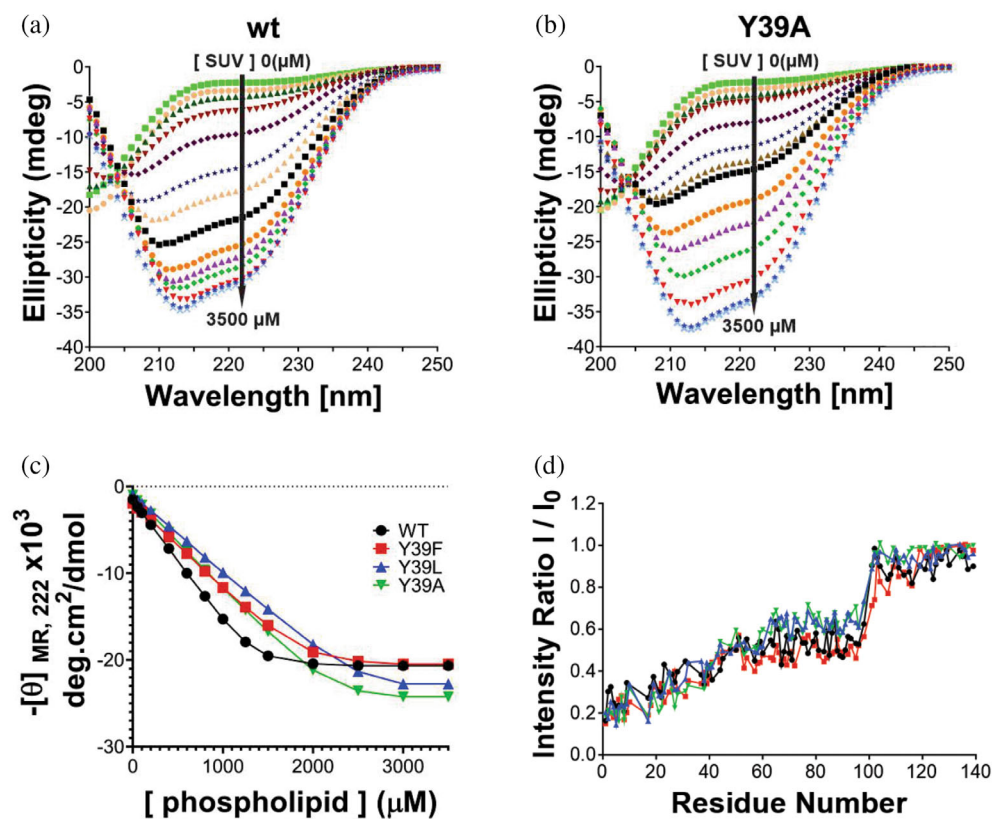


**FIGURE 4** Effect of Y39 mutations on the membrane binding features of  $\alpha$ S. (a–b) cd spectra of wt (a) and Y39A  $\alpha$ S (b) species with increasing concentrations of SUVs (0 to 3.5 mM). (c) Data from  $\theta_{MR,222}$  in wt  $\alpha$ S and its Y39F, Y39L, and Y39A variants as a function of lipid concentration were fit to Equation 2 to calculate  $K_d$  values. (d) Graphs of  $I/I_0$  (where  $I$  and  $I_0$  are the peak intensities observed in the presence and absence of SUVs, respectively) plotted against residue number for wt  $\alpha$ S and its Y39F, Y39L, and Y39A variants

**TABLE 1** Fractional populations of membrane-bound  $\alpha$ S conformers determined by NMR

Variant	Total bound <sup>a,b</sup>	Hidden <sup>a,c</sup>	Exposed <sup>a,d</sup>
wt	0.72	0.57	0.15
Y39F	0.71	0.56	0.15
Y39L	0.74	0.49	0.25
Y39A	0.70	0.40	0.30

<sup>a</sup>Values were determined from 2D  $^1\text{H}$ - $^{15}\text{N}$ -HSQC data in Figure 4 and are expressed as a fraction of the total protein. Each sample consisted of a mixture of  $\alpha$ S and phospholipids at concentrations of 100  $\mu\text{M}$  and 2.5 mM, respectively.

<sup>b</sup>Determined from the mean attenuation of residues 3–9 (i.e., total bound =  $1 - \{I/I_0\}_{\text{mean},3-9}$ ).<sup>28,44</sup>

<sup>c</sup>Determined from the mean attenuation of residues 66–80 (i.e., hidden =  $1 - \{I/I_0\}_{\text{mean},66-80}$ ).<sup>28,44</sup>

<sup>d</sup>Calculated as the difference between the total bound population and the hidden population.<sup>28,44</sup>

39 regulates lipid membrane interactions involving the central hydrophobic NAC domain.

### 3 | DISCUSSION

Overall, the results presented here demonstrate that aromaticity at position 39 of  $\alpha$ S might play a crucial role in molecular events that might represent functional or

dysfunctional states of  $\alpha$ S. In that direction, a recent study revealed that the aggregation of  $\alpha$ S is regulated by specific sequence motifs flanking the NAC region.<sup>27,32</sup> The pre-NAC segment  $^{36}\text{GVLYVGS}^{42}$  was suggested to be a critical requirement for  $\alpha$ S aggregation in vivo, whereas removal of this motif prevented  $\alpha$ S aggregation and also suppressed the aggregation-induced toxicity in vivo.<sup>27,32</sup> However, certain questions remained unanswered, such as what is the significance of individual residues in that sequential motif in modulating the aggregation of  $\alpha$ S. Our findings point to the significance of aromaticity in the  $^{36}\text{GVLYVGS}^{42}$  motif as a key factor determining the amyloid fibril assembly of  $\alpha$ S. The substantial change of aggregation rate on passing from wt  $\alpha$ S to the Y39A and the Y39L variants might be attributable to a loss of function of the aromatic side chain in the self-assembly process and/or to a conformational stabilization of the native state.

Added to that, our findings also indicate that the aromatic character at position 39 of  $\alpha$ S favors a NAC membrane-anchored state for the lipid-bound conformation of  $\alpha$ S, supporting further a role for Tyr-39 as a factor aiding in the folding of the amphiphilic region and promoting helix propagation.<sup>29</sup> Interestingly, it was proposed recently that the equilibrium between membrane-bound and unbound states of the region 65–97, which overlaps with the NAC region, might play a role in the regulation

of biological properties of  $\alpha$ S.<sup>43</sup> Indeed, transition toward partly helical membrane-bound states of  $\alpha$ S has been associated with the control of vesicle docking and/or protein–protein interactions mediated by  $\alpha$ S via a double-anchor mechanism.<sup>43</sup> In line with this hypothesis, phosphorylation of  $\alpha$ S at Tyr-39 was shown to promote partly helical membrane-bound states.<sup>26</sup> Accordingly, it was suggested that in the cellular context, alternation of  $\alpha$ S between its two membrane-bound states might be driven by phosphorylation at Tyr-39, which would play then a role as a conformational switch.<sup>26</sup>

Remarkably, the region encompassing residues 34–45 of  $\alpha$ S has been identified as a ganglioside-binding domain<sup>45</sup> which are specific of outer plasma membrane leaflets and are related to cellular uptake of  $\alpha$ S monomers<sup>46</sup> and its pathological aggregates.<sup>47,48</sup> In that domain, Tyr-39 was shown to be the most critical residue for the interaction. In line with our findings, the work concluded that it is not Y39 per se the residue responsible for the recognition of the lipid domain but the presence of an aromatic moiety at this position.<sup>46</sup>

Interestingly, a lipid-chaperone hypothesis was recently proposed, in which the amyloidogenic protein–lipid complex plays the role of the main actor in membrane damage.<sup>49</sup> In that context, the lipid–protein complexes rather than the bare proteins are considered the key players in membrane damage. Considering that aggregation and membrane damage is an important driver of cellular toxicity in amyloid diseases, future work is needed to link our findings with studies based on toxicity and neuronal cell death.

## 4 | MATERIALS AND METHODS

### 4.1 | Protein and reagents

Unlabeled and <sup>15</sup>N isotopically enriched N-terminally acetylated  $\alpha$ S and its Y39F, Y39L, and Y39A variants were obtained by co-transforming *E. coli* BL21 cells with the plasmid harboring the corresponding protein gene and a second one that encodes for the components of yeast NatB acetylase complex.<sup>50</sup> Both plasmids carried different antibiotic resistance, namely, Ampicillin and Chloramphenicol to select the doubly transformed *E. coli* colonies. Purification was carried out as previously reported,<sup>15</sup> with the exception that when required, both antibiotics were included in the growth flasks to avoid plasmid purge during growth and expression. The final purity of the protein samples was determined by SDS-PAGE. Purified protein samples were dissolved in 20 mM MES buffer supplemented with 100 mM NaCl at pH 6.5 (Buffer A). <sup>15</sup>N NH<sub>4</sub>Cl was purchased from Cambridge Isotope

Laboratories, and MES buffer and D<sub>2</sub>O were purchased from Merck or Sigma. Protein concentrations were determined spectrophotometrically by measuring absorption at 274 nm and using an epsilon value of 5,600 M<sup>-1</sup> cm<sup>-1</sup>.

### 4.2 | Aggregation assay

Aggregation kinetics measurements were performed with 50  $\mu$ M protein samples dissolved in Buffer A, which were incubated at 37°C under constant stirring. To perform the aggregation studies, we used an NMR-based approach that measures the consumption of the monomeric state of the amyloid protein during the progression of the aggregation process.<sup>51,52</sup> The amount of soluble  $\alpha$ S monomers at different time points of the aggregation assay was determined by integration of the protein NMR resonances in the aliphatic region of the one-dimensional (1D) <sup>1</sup>H NMR spectrum (0.7–1.0 ppm). Acquisition and processing of NMR spectra were performed using TOPSPIN 7.0 (Bruker Biospin). In addition, endpoint aliquots of aggregation assays were analyzed by the Thioflavin-T (ThT) fluorescence assay<sup>53</sup> and CD spectroscopy.<sup>42</sup>

### 4.3 | Electron microscopy

Ten-microliter aliquots withdrawn from aggregation reactions were adsorbed onto Formvar/carbon-coated copper grids (Pella, Redding, CA) and negative stained with 2% (w/v) uranyl acetate. Images were obtained at various magnifications (1,000–90,000X) using a Philips CM120 transmission electron microscope.

### 4.4 | AFM microscopy

Samples were prepared by spin-coating. A volume 20  $\mu$ L of each sample was deposited over Muscovite mica discs grade V1 (Ted Pella) of 10 mm diameter, which were previously cleaved. After promoting interactions with the substrate, mica discs were accelerated up to a constant rotation speed of 2000 rpm to ensure complete drying of the substrate. AFM imaging was performed on a Bruker Multimode 8 SPM (Santa Barbara, CA, USA) and a NanoScope V Controller (Santa Barbara, CA, USA) using a “J” type scanner. The AFM images were acquired in tapping mode using silicon tips NCHV (Bruker) with a spring constant of 40 N m<sup>-1</sup> and a resonance frequency of  $\sim$ 320 kHz. Images analyses were performed using Gwyddion version 2.46 software (Brno, Czech Republic).<sup>54</sup>

## 4.5 | Preparation of SUVs

1,2-Dioleoyl-sn-glycero-3-phosphoethanol-amine (DOPE), 1,2-dioleoyl-sn-glycero-3-phospho-L-serine (DOPS), and 1,2-dioleoyl-sn-glycero-3-phosphocholine (DOPC) were purchased from Avanti Polar Lipids (Alabaster, AL), as pure DOPC and a DOPE/DOPS/DOPC mixture with a 5:3:2 weight ratio (Coagulation Reagent I). Phospholipid mixtures containing Coagulation Reagent I or 60% DOPC, 25% DOPE, and 15% DOPS (molar concentrations) were prepared by drying a mixture of the different lipids dissolved in chloroform under a stream of N<sub>2</sub> gas and re-suspending the lipid film in Buffer A.<sup>55</sup> SUVs were prepared by pulse-sonicating the phospholipid suspensions in a bath sonicator (10 cycles of 2 min with separation of 2 min). The size of the resulting SUVs (hydrodynamic radii of 40–50 nm) was determined by dynamic light scattering using a Zetasizer Nano ZS instrument (Malvern Instruments, Worcestershire, U.K.).

## 4.6 | Far-UV circular dichroism (CD)

The content of  $\alpha$ -helix structure of  $\alpha$ S monomer upon binding to SUVs was evaluated by far-UV circular dichroism (CD). Solutions of 10  $\mu$ M of  $\alpha$ S monomer in the absence or presence of varying concentration of SUVs were analyzed at 25°C (SUV composition: 20% DOPC, 50% DOPE, and 30% DOPS). Far-UV CD spectra were recorded from 200 to 250 nm in a J-1500 CD spectrophotometer (JASCO, Inc.), using a 0.1 cm quartz cuvette (bandwidth = 1 nm; scan rate = 50 nm/min; accumulation = 3).

The ellipticity at 222 nm was measured and the background associated with buffer or SUV solutions was subtracted. The mean residue molar ellipticity at 222 nm ( $[\theta]_{MR,222}$ ) was calculated using Equation 1:

$$[\theta]_{MR,222} = \theta_{222} / (10Cnl) \quad (1)$$

where  $\theta_{222}$  is the measured ellipticity (millidegrees) at 222 nm,  $C$  is the protein concentration (molar),  $n = 140$  (number of amino acid residues in the protein), and  $l$  is the path length of the cuvette in cm (0.1 cm). Lipid titration curves generated by plotting  $[\theta]_{MR,222}$  versus the lipid concentration were analyzed by fitting to Equation 2, as previously described<sup>44</sup>:

$$R = R_0 - (R_0 - R_f) \frac{K_d + C + L/N - \sqrt{(K_d + C + L/N)^2 - 4CL/N}}{2C} \quad (2)$$

where  $R$  is the measured  $\theta_{MR,222}$  at a given lipid concentration,  $R_0$  is the  $\theta_{MR,222}$  in the absence of lipid,  $R_f$  is the  $\theta_{MR,222}$  in the presence of saturating lipid,  $L$  is the total lipid concentration,  $C$  is the total protein concentration,  $K_d$  is the apparent macroscopic dissociation equilibrium constant, and  $N$  is the binding stoichiometry (lipids/protein).

## 4.7 | NMR spectroscopy of the interaction with lipid vesicles

NMR spectra were recorded on a Bruker 600 MHz HD Advance III spectrometer, equipped with a cryogenically cooled triple resonance <sup>1</sup>H (<sup>13</sup>C/<sup>15</sup>N) TCI probe. Two-dimensional 2D <sup>1</sup>H–<sup>15</sup>N HSQC experiments were recorded at 15°C using standard pulse sequences from the Topspin suite (Bruker) library. Sequence-specific assignments for the backbone of the intrinsically unfolded  $\alpha$ S were obtained from our previous works. In the case of the Y39A, Y39F, and Y39L mutants, assignment of backbone resonances in the vicinity of the mutation was confirmed by 3D TOCSY-HSQC and NOESY-HSQC experiments. Binding of monomers of  $\alpha$ S and its Y39F, Y39L, and Y39A variants to SUVs was determined via 2D <sup>1</sup>H–<sup>15</sup>N HSQC experiments in which 100  $\mu$ M <sup>15</sup>N-labeled  $\alpha$ S species in Buffer A, 10% D<sub>2</sub>O, was incubated in the absence or the presence of 2.5 mM SUVs (SUV composition: 60% DOPC, 25% DOPE, and 15% DOPS). To monitor residue-specific interactions of  $\alpha$ S variants with SUVs, the fractional signal attenuation of each residue peak was determined by comparing their intensities in the presence ( $I$ ) and absence of SUVs ( $I_0$ ), as previously described.<sup>40</sup> The  $I/I_0$  ratios of non-overlapping cross-peaks were plotted as a function of the protein sequence to obtain the protein–lipid interaction profiles. The fractional population of molecules bound to the membrane (“total bound population”) was determined from the mean attenuation of residues 3–9<sup>28,44</sup> (Table 1). Regarding the conformation of the hydrophobic domain NAC at the membrane surface, in the fractional population of protein in the associated state (referred to here as “hidden”), we determined the mean attenuation of residues 66–80<sup>28,44</sup> (Table 1). The fractional population of protein with residues 66–80 in the dissociated state (referred to here as “exposed”) was determined by subtracting the hidden population from the total bound population (residues 3–9).<sup>28,44</sup> (Table 1). Acquisition and processing of NMR spectra were performed using TOPSPIN 7.0 (Bruker Biospin). 2D spectra analysis and visualization were performed with CCPN.



## 4.8 | Cell-based assay

### 4.8.1 | Cell culture and transfection

For the studies with cell-based models of  $\alpha$ S aggregation, H4 neuroglioma cells were maintained at 5% CO<sub>2</sub> and 37°C in Dulbecco's Modified Eagle's Medium (DMEM) (Gibco) supplemented with 10% fetal bovine serum and 1% Penicillin Streptomycin. One day before the transfection, cells were seeded in 12-well plates. Cells were co-transfected with plasmids encoding a C-terminally modified variant of  $\alpha$ S or its point mutants (SynT construct) and synphilin-1<sup>38</sup> using FuGene (Promega), according to the manufacturer's instructions. Inclusion formation was assessed 48 hr post-transfection.

### 4.8.2 | Immunocytochemistry

Cells were fixed with 4% paraformaldehyde in PBS 48 hr after transfection. For permeabilization, cells were treated with 0.1% Triton X-100 and blocked with 1.5% bovine serum albumin (BSA) in PBS. Cells were then incubated with anti- $\alpha$ S primary antibody (BD 610787, 1:1000) and anti-V5 tag (Abcam ab9116, 1:100), either 4 hr at room temperature or overnight at 4°C, and 1 hr in Alexa Fluor 488 donkey anti-rabbit and Alexa Fluor 555 donkey anti-mouse as secondary antibodies (Invitrogen A21202 and A31570, respectively, 1:1000). Cells were further stained with DAPI (Sigma, D9542) for 5–10 min. Images were captured using a Nikon C2 Plus confocal microscope.

### 4.8.3 | Quantification of $\alpha$ S intracellular inclusions

Transfected cells were detected and scored based on the pattern of  $\alpha$ S intracellular inclusions, by classifying them into four groups: cells without inclusions, less than five inclusions (<5 inclusions), between five to nine inclusions (5–9 inclusions), and equal/more than ten inclusions ( $\geq$ 10 inclusions).<sup>38</sup> Results were expressed as the percentage of the total number of transfected cells obtained from three independent experiments. At least 50–100 cells were counted per condition.

### 4.8.4 | Western blot analysis

H4 cells were lysed with radio-immunoprecipitation assay (RIPA) lysis buffer (50 mM Tris pH 8.0, 0.15 M

NaCl, 0.1% SDS, 1% NP40, 0.5% Na-deoxycholate) and 2 mM EDTA and supplemented with a Protease Inhibitor Cocktail (Roche Diagnostics, Mannheim, Germany). Protein concentration was determined using the Bradford assay (BioRad Laboratories, Hercules, CA, USA) and the gels were loaded with 40  $\mu$ g protein after denaturation for 5 min at 100°C in SDS-PAGE protein sample buffer. The samples were separated on 12% SDS-polyacrylamide gels (SDS-PAGE). The transfer was carried out to nitrocellulose membrane (Amersham™ Hybond®, GE Healthcare Life Sciences) for 90 min with constant current at 0.3 A and 4°C, using Tris-Glycine transfer buffer. Membranes were fixed in 8% para-formaldehyde and blocked with 5% (w/v) skim milk in 1xTBS-Tween (50 mM Tris, 150 mM NaCl, 0.05% Tween, pH 7.5) for 60 min at room temperature. Membranes were further incubated with the primary antibody, mouse anti-ASYN (1:1000, 2B2D1 BD Biosciences, San Jose, CA, USA), and mouse anti- $\alpha$ tubulin (T6199, Sigma-Aldrich) overnight at 4°C. After washing three times in TBS-Tween for 5 min, membranes were incubated for 1 hr with secondary antibody, anti-mouse IgG (A4416, Sigma-Aldrich). Detection was carried out by chemiluminescence (Bio-Lumina; Kalium Technologies, Argentina) using a Licor C-Digit Blot Scanner (LI-COR Biosciences) according to the manufacturer instructions.

## 4.9 | *C. elegans* study

### 4.9.1 | Strains

All strains were grown on Agar plates containing OP50 bacteria at 20°C as described previously.<sup>56</sup> Transgenic animals expressing  $\alpha$ S from an extra-chromosomal array were generated by injecting wild-type Bristol N<sub>2</sub> worms with plasmids expressing different forms of human  $\alpha$ S with mCherry fused to its C-terminus. Mutations in  $\alpha$ S (Y39F, Y39L, Y39A) were introduced by mutagenesis PCR and validated by sequencing. The protein  $\alpha$ S was expressed in neuronal cells of *C. elegans* under the control of the pan-neuronal *rab-3* promoter (*rab-3p: $\alpha$ S-mCherry*) using the expression vector pD115.62 as a backbone. To generate transgenic lines, the gonads of young adult N<sub>2</sub> worms have been injected with a plasmid mix containing 50 ng/ $\mu$ l *rab-3p: $\alpha$ S-mCherry*, 5 ng/ $\mu$ l of a co-injection marker (*myo-2p::mTFP*), and 45 ng/ $\mu$ l pBluescript KSII (Stratagene) to reach a final DNA concentration of 100 ng/ $\mu$ l, as described previously.<sup>57</sup>

### 4.9.2 | Fluorescent imaging and analysis

Young adult *C. elegans* were mounted on a 2% agarose pad and immobilized by 50 mM sodium azide in M9

buffer (17.2 mM  $\text{KH}_2\text{PO}_4$ , 42.3 mM  $\text{Na}_2\text{HPO}_4$ , 85.6 mM NaCl, 1 mM  $\text{MgSO}_4$ ). Z-stacks of the neuronal cell bodies were taken on a Zeiss LSM 780 confocal microscope with a 63x/1.40 NA oil immersion objective. Projections of the stacks and statistical analysis have been carried out with ImageJ 2.1.0 and Prism Version 5.03.

#### 4.9.3 | Western blotting

About 100  $\alpha\text{S}$  expressing worms were washed twice in ice cold PBS (137 mM NaCl, 2.7 mM KCl, 10 mM  $\text{Na}_2\text{HPO}_4$ , 1.8 mM  $\text{KH}_2\text{PO}_4$ ) with phosphatase and protease inhibitors (PhosphoStop Phosphatase Inhibitor Cocktail Tablets (Roche), complete EDTA-free Protease Inhibitor Cocktail Tablets (Roche)) and lysed in 60  $\mu\text{L}$  lysis buffer (150 mM NaCl, 1 mM EDTA, 25 mM Tris pH 7.5, 10% (v/v) glycerol, 1% (v/v) Triton X and with freshly added 100 mM DTT, 4 mM Pefabloc SC-Protease Inhibitor (A 154.1, Roth), Phosphostop Phosphatase Inhibitor Cocktail Tablets (Roche), and complete EDTA-free Protease Inhibitor Cocktail Tablets (Roche)) prior to shock-freezing in liquid nitrogen. Samples were directly transferred to  $-80^\circ\text{C}$ . After thawing, SDS-PAGE protein sample buffer was added. Subsequently, the samples were sonicated on ice for 3 min (20 sec on, 10 sec off, 70% amplitude) with an SonoPlus mini20 Sonicator (3,665, Bandelin, Sonotrode Type MS2.5). After boiling at  $100^\circ\text{C}$  for 10 min, the lysate was centrifuged at 17000 g for 10 min. About 30  $\mu\text{L}$  of the lysate has been separated on 12% SDS-polyacrylamide gels and subsequently transferred to a PVDF membrane (10,600,023, Amersham Hybond) for 90 min at 220 mA under cooling conditions. Membranes were blocked with 1% semi-skimmed milk in 1% TBS-T buffer (20 mM Tris, 150 mM NaCl, 0.1% (v/v) Tween 20, pH 7.6) for 1 hr. Primary antibody incubation was performed in blocking solution with mouse anti- $\alpha\text{S}$  (1:1000, 610,787, BD Transduction Laboratories) or mouse anti- $\alpha\text{tubulin}$  (1:2000, T6199, Sigma-Aldrich) overnight, with agitation at  $4^\circ\text{C}$ . Next, membranes were washed 3 times in TBS-T buffer for 7 min and incubated at room temperature with agitation in (goat) anti-mouse HRP-conjugated secondary antibody in blocking solution (1:5000, 1,721,011, Bio-RAD Laboratories, Inc.). For the detection of the chemiluminescence, the ECL Kit Prime Western Blotting Detection Reagents (RPN2232, Amersham) and an Intas ChemoCam Imager were used according to the manufacturer's instructions.

#### AUTHOR CONTRIBUTIONS

**Fiamma A. Buratti:** Conceptualization (equal); data curation (equal); formal analysis (equal); investigation (equal); writing – original draft (equal); writing – review

and editing (equal). **Nicola Boeffinger:** Formal analysis (equal); investigation (equal). **Hugo A. Garro:** Formal analysis (equal); investigation (equal). **Jesica S. Flores:** Formal analysis (equal); investigation (equal). **Francisco J. Hita:** Formal analysis (equal); investigation (equal). **Phelippe do Carmo Gonçalves:** Formal analysis (equal); investigation (equal). **Federico dos Reis Copello:** Formal analysis (equal); investigation (equal). **Leonardo Lizarraga:** Formal analysis (equal); investigation (equal). **Giulia Rossetti:** Formal analysis (equal); investigation (equal). **Paolo Carloni:** Formal analysis (equal); supervision (equal); writing – original draft (equal). **Markus Zweckstetter:** Formal analysis (equal); supervision (equal); writing – original draft (equal). **Tiago F. Outeiro:** Formal analysis (equal); writing – original draft (equal). **Stefan Eimer:** Formal analysis (equal); supervision (equal); writing – original draft (equal). **Christian Griesinger:** Formal analysis (equal); supervision (equal); writing – original draft (equal). **Claudio Oscar Fernandez:** Conceptualization (lead); formal analysis (lead); funding acquisition (lead); investigation (lead); methodology (lead); project administration (lead); resources (lead); supervision (lead); validation (lead); writing – original draft (lead); writing – review and editing (lead).

#### ACKNOWLEDGMENTS

C.O.F. thanks Universidad Nacional de Rosario (UNR) and ANPCyT-FONCyT (PICT 2014-3704 and PICT 2017-4665) for financial support. C.O.F. and C.G. thank the Max Planck Society (P10390) for support. F.A.B. thanks CONICET for fellowship. TFO is supported by the Deutsche Forschungsgemeinschaft (DFG, German Research Foundation) under Germany's Excellence Strategy - EXC 2067/1- 390729940, and SFB1286 (Project B8). M.Z. was supported by the EU Horizon 2020 research and innovation program (grant agreement No. 787679) and by The Michael J. Fox Foundation for Parkinson's Research (Grant ID: MJFF-019033). Open Access funding enabled and organized by Projekt DEAL.

#### CONFLICTS OF INTEREST

There are no conflicts to declare.

#### ORCID

Claudio O. Fernández  <https://orcid.org/0000-0003-0454-7735>

#### REFERENCES

1. Maroteaux L, Campanelli JT, Scheller RH. Synuclein: A neuron-specific protein localized to the nucleus and presynaptic nerve terminal. *J Neurosci*. 1988;8(8):2804–2815.
2. Fanciulli A, Wenning GK. Multiple-system atrophy. *N Engl J Med*. 2015;372(3):249–263.

3. Gómez-Tortosa E, Newell K, Irizarry MC, Sanders JL, Hyman BT.  $\alpha$ -Synuclein Immunoreactivity in dementia with Lewy bodies: Morphological staging and comparison with ubiquitin immunostaining. *Acta Neuropathol.* 2000;99(4):352–357.
4. Irwin DJ, Lee VM, Trojanowski JQ. Amyloid Beta-peptide and the dementia of Parkinson's disease. *Nat Rev Neurosci.* 2013;14(9):626–636.
5. Luk KC, Lee VMY. Modeling Lewy pathology propagation in Parkinson's disease. *Parkinsonism Relat Disord.* 2014;20(01):S85–S87.
6. McCann H, Stevens CH, Cartwright H, Halliday GM.  $\alpha$ -Synucleinopathy phenotypes. *Parkinsonism Relat Disord.* 2014;20(1):S62–S67.
7. Spillantini MG, Crowther RA, Jakes R, Hasegawa M, Goedert M.  $\alpha$ -Synuclein in filamentous inclusions of Lewy bodies from Parkinson's disease and dementia with Lewy bodies. *Proc Natl Acad Sci U S A.* 1998;95(11):6469–6473.
8. Spillantini MG, Schmidt ML, Lee VMY, Trojanowski JQ, Jakes R, Goedert M.  $\alpha$ -Synuclein in Lewy Bodies. *Nature.* 1997;388(6645):839–840.
9. Watson JB, Hatami A, David H, et al. Alterations in Corticostriatal synaptic plasticity in mice overexpressing human  $\alpha$ -Synuclein. *Neuroscience.* 2009;159(2):501–513.
10. Cooper AA, Gitler AD, Cashikar A, et al.  $\alpha$ -Synuclein blocks ER-Golgi traffic and Rab1 rescues neuron loss in Parkinson's models. *Science.* 2006;313(5785):324–328.
11. Vargas KJ, Makani S, Davis T, Westphal CH, Castillo PE, Chandra SS. Synucleins regulate the kinetics of synaptic vesicle endocytosis. *J Neurosci.* 2014;34(28):9364–9376.
12. Bussell R, Eliezer D. A structural and functional role for 11-Mer repeats in  $\alpha$ -Synuclein and other exchangeable lipid binding proteins. *J Mol Biol.* 2003;329(4):763–778.
13. Du HN, Tang L, Luo XY, et al. A peptide motif consisting of glycine, alanine, and valine is required for the fibrillization and cytotoxicity of human  $\alpha$ -Synuclein. *Biochemistry.* 2003;42(29):8870–8878.
14. Giasson BI, Murray IVJ, Trojanowski JQ, Lee VMY. A hydrophobic stretch of 12 amino acid residues in the middle of  $\alpha$ -Synuclein is essential for filament assembly. *J Biol Chem.* 2001;276(4):2380–2386.
15. Hoyer W, Cherny D, Subramaniam V, Jovin TM. Impact of the acidic C-terminal region comprising amino acids 109–140 on  $\alpha$ -Synuclein aggregation in vitro. *Biochemistry.* 2004;43(51):16233–16242.
16. Kim TD, Paik SR, Yang CH. Structural and functional implications of C-terminal regions of  $\alpha$ -Synuclein. *Biochemistry.* 2002;41(46):13782–13790.
17. Sang MP, Han YJ, Kim TD, Jeon HP, Yang CH, Kim J. Distinct roles of the N-terminal-binding domain and the C-terminal-solubilizing domain of  $\alpha$ -Synuclein, a molecular chaperone. *J Biol Chem.* 2002;277(32):28512–28520.
18. Bertocini CW, Jung YS, Fernandez CO, et al. Release of Long-range tertiary interactions potentiates aggregation of natively unstructured  $\alpha$ -Synuclein. *Proc Natl Acad Sci U S A.* 2005;102(5):1430–1435.
19. Cho MK, Nodet G, Kim HY, et al. Structural characterization of  $\alpha$ -Synuclein in an aggregation prone state. *Protein Sci.* 2009;18(9):1840–1846.
20. Dedmon MM, Lindorff-Larsen K, Christodoulou J, Vendruscolo M, Dobson CM. Mapping Long-range interactions in  $\alpha$ -Synuclein using spin-label NMR and ensemble molecular dynamics simulations. *J Am Chem Soc.* 2005;127(2):476–477.
21. Eliezer D, Kutluay E, Bussell R, Browne G. Conformational properties of  $\alpha$ -Synuclein in its free and lipid-associated states. *J Mol Biol.* 2001;307(4):1061–1073.
22. Aspholm EE, Matečko-Burmann I, Burmann BM. Keeping  $\alpha$ -Synuclein at bay: A more active role of molecular chaperones in preventing mitochondrial interactions and transition to pathological states? *Life.* 2020;10(11):1–19.
23. Brahmachari S, Karuppagounder SS, Ge P, et al. C-Abl and Parkinson's disease: Mechanisms and therapeutic potential. *J Parkinsons Dis.* 2017;7(4):589–601.
24. Burai R, Ait-Bouziad N, Chiki A, Lashuel HÁ. Elucidating the role of site-specific nitration of  $\alpha$ -Synuclein in the pathogenesis of Parkinson's disease via protein Semisynthesis and mutagenesis. *J Am Chem Soc.* 2015;137(15):5041–5052.
25. Burmann BM, Gerez JA, Matečko-Burmann I, et al. Regulation of  $\alpha$ -Synuclein by chaperones in mammalian cells. *Nature.* 2020;577(7788):127–132.
26. Dikiy I, Fauvet B, Jovičić A, et al. Semisynthetic and in vitro phosphorylation of alpha-Synuclein at Y39 promotes functional partly helical membrane-bound states resembling those induced by PD mutations. *ACS Chem Biol.* 2016;11(9):2428–2437.
27. Doherty CPA, Ulamec SM, Maya-Martinez R, et al. A short motif in the N-terminal region of  $\alpha$ -Synuclein is critical for both aggregation and function. *Nat Struct Mol Biol.* 2020;27:249–259.
28. Lima VDA, Do Nascimento LA, Eliezer D, Follmer C. Role of Parkinson's disease-linked mutations and N-terminal acetylation on the Oligomerization of  $\alpha$ -Synuclein induced by 3,4-Dihydroxyphenylacetaldehyde. *ACS Chem Neurosci.* 2019;10(1):690–703.
29. Lokappa SB, Suk JE, Balasubramanian A, Samanta S, Situ AJ, Ulmer TS. Sequence and membrane determinants of the random coil-helix transition of  $\alpha$ -Synuclein. *J Mol Biol.* 2014;426(10):2130–2144.
30. Mahul-Mellier AL, Fauvet B, Gysbers A, et al. C-Abl phosphorylates  $\alpha$ -Synuclein and regulates its degradation: Implication for  $\alpha$ -Synuclein clearance and contribution to the pathogenesis of Parkinson's disease. *Hum Mol Genet.* 2014;23(11):2858–2879.
31. Sevcsik E, Trexler AJ, Dunn JM, Rhoades E. Allosteric in a disordered protein: Oxidative modifications to  $\alpha$ -Synuclein act distally to regulate membrane binding. *J Am Chem Soc.* 2011;133(18):7152–7158.
32. Tripathi TA. Master regulator of  $\alpha$ -Synuclein aggregation. *ACS Chem Neurosci.* 2020;11(10):1376–1378.
33. Uversky VN, Yamin G, Munishkina LA, et al. Effects of nitration on the structure and aggregation of  $\alpha$ -Synuclein. *Mol Brain Res.* 2005;134(1):84–102.
34. Zhao K, Lim YJ, Liu Z, et al. Parkinson's disease-related phosphorylation at Tyr39 rearranges  $\alpha$ -Synuclein amyloid fibril structure revealed by Cryo-EM. *Proc Natl Acad Sci U S A.* 2020;117(33):20305–20315.
35. Lamberto GR, Binolfi A, Orcellet ML, et al. Structural and mechanistic basis behind the inhibitory interaction of PcTS on

- $\alpha$ -Synuclein amyloid fibril formation. *Proc Natl Acad Sci U S A*. 2009;106(50):21057–21062.
36. Lamberto GR, Torres-Monserrat V, Bertocini CW, et al. Toward the discovery of effective polycyclic inhibitors of  $\alpha$ -Synuclein amyloid assembly. *J Biol Chem*. 2011;286(37):32036–32044.
37. Palomino-Hernandez O, Buratti FA, Sacco PS, Rossetti G, Carloni P, Fernandez CO. Role of Tyr-39 for the structural features of  $\alpha$ -Synuclein and for the interaction with a strong modulator of its amyloid assembly. *Int J Mol Sci*. 2020;21(14):1–16.
38. Lázaro DF, Rodrigues EF, Langohr R, et al. Systematic comparison of the effects of alpha-Synuclein mutations on its Oligomerization and aggregation. *PLoS Genet*. 2014;10(11):e1004741.
39. Karpinar DP, Balija MBG, Kügler S, et al. Pre-Fibrillar  $\alpha$ -Synuclein variants with impaired B-structure increase neurotoxicity in Parkinson's disease models. *EMBO J*. 2009;28(20):3256–3268.
40. Bodner CR, Maltsev AS, Dobson CM, Bax A. Differential phospholipid binding of  $\alpha$ -synuclein variants implicated in Parkinson's disease revealed by solution NMR spectroscopy. *Biochemistry*. 2010;49:862–871.
41. Bartels T, Ahlstrom LS, Leftin A, et al. The N-terminus of the intrinsically disordered protein  $\alpha$ -synuclein triggers membrane binding and helix folding. *Biophys J*. 2010;99:2116–2124.
42. Fonseca-Ornelas L, Eisbach SE, Paulat M, et al. Small molecule-mediated stabilization of vesicle-associated helical  $\alpha$ -Synuclein inhibits pathogenic Misfolding and aggregation. *Nat Commun*. 2014;5:5857.
43. Man WK, Tahirbegi B, Vrettas MD, et al. The docking of synaptic vesicles on the presynaptic membrane induced by  $\alpha$ -Synuclein is modulated by lipid composition. *Nat Commun*. 2021;12(1):927.
44. Ysselstein D, Joshi M, Mishra V, et al. Effects of impaired membrane interactions on  $\alpha$ -Synuclein aggregation and neurotoxicity. *Neurobiol Dis*. 2015;79:150–163.
45. Fantini J, Yahi N. Molecular basis for the glycosphingolipid-binding specificity of  $\alpha$ -Synuclein: Key role of tyrosine 39 in membrane insertion. *J Mol Biol*. 2011;408(4):654–669.
46. Park JY, Kim KS, Lee SB, et al. On the mechanism of internalization of  $\alpha$ -Synuclein into microglia: Roles of ganglioside GM1 and lipid raft. *J Neurochem*. 2009;110(1):400–411.
47. Fusco G, Chen SW, Williamson PTF, et al. Structural basis of membrane disruption and cellular toxicity by A-Synuclein oligomers. *Science*. 2017;358(6369):1440–1443.
48. Masaracchia C, Hnida M, Gerhardt E, et al. Membrane binding, internalization, and sorting of alpha-Synuclein in the cell. *Acta Neuropathol Commun*. 2018;6(1):79.
49. Sciacca MF, Lolicato F, Tempra C, et al. Lipid-chaperone hypothesis: A common molecular mechanism of membrane disruption by intrinsically disordered proteins. *ACS Chem Neurosci*. 2020;11(24):4336–4350.
50. Miotto MC, Rodriguez EE, Valiente-Gabioud AA, et al. Site-specific copper-catalyzed oxidation of  $\alpha$ -Synuclein: Tightening the link between metal binding and protein oxidative damage in Parkinson's disease. *Inorg Chem*. 2014;53(9):4350–4358.
51. Binolfi A, Rodriguez EE, Valensin D, et al. Bioinorganic chemistry of Parkinson's disease: Structural determinants for the copper-mediated amyloid formation of alpha-Synuclein. *Inorg Chem*. 2010;49(22):10668–10679.
52. Valiente-Gabioud AA, Riedel D, Outeiro TF, Menacho-Márquez MA, Griesinger C, Fernández CO. Binding modes of Phthalocyanines to amyloid  $\beta$  peptide and their effects on amyloid fibril formation. *Biophys J*. 2018;114(5):1036–1045.
53. Fernández CO, Hoyer W, Zweckstetter M, et al. NMR of  $\alpha$ -Synuclein-polyamine complexes elucidates the mechanism and kinetics of induced aggregation. *EMBO J*. 2004;23(10):2039–2046.
54. Nečas D, Klapetek P. Gwyddion: An open-source software for SPM data analysis. *Centr Eur J Phys*. 2012;10(1):181–188.
55. Maltsev AS, Ying J, Bax A. Impact of N-terminal acetylation of  $\alpha$ -Synuclein on its random coil and lipid binding properties. *Biochemistry*. 2012;51(25):5004–5013.
56. Brenner S. The genetics of *Caenorhabditis Elegans*. *Genetics*. 1974;77(1):71–94.
57. Mello CC, Kramer JM, Stinchcomb D, Ambros V. Efficient gene transfer in *C.Elegans*: Extrachromosomal maintenance and integration of transforming sequences. *EMBO J*. 1991;10(12):3959–3970.

## SUPPORTING INFORMATION

Additional supporting information can be found online in the Supporting Information section at the end of this article.

**How to cite this article:** Buratti FA, Boeffinger N, Garro HA, Flores JS, Hita FJ, Gonçalves PC, et al. Aromaticity at position 39 in  $\alpha$ -synuclein: A modulator of amyloid fibril assembly and membrane-bound conformations. *Protein Science*. 2022;31(7):e4360. <https://doi.org/10.1002/pro.4360>